

# A Mysteriously Tight H $\alpha$ -[O III] Correlation and Non-Case B Balmer Decrements Revealed by the Spectra from the James Webb Space Telescope NIRSpec Instrument

BANGZHENG SUN<sup>1</sup> AND HAOJING YAN<sup>1</sup>

<sup>1</sup>*Department of Physics and Astronomy, University of Missouri - Columbia  
701 S College Avenue  
Columbia, MO 65201, USA*

## ABSTRACT

We report an extremely tight, linear relation between H $\alpha$  and [O III] line fluxes in logarithm, discovered using a large sample of low and mid-resolution spectra (totaling 563) obtained by the James Webb Space Telescope (JWST) NIRSpec instrument in three widely separated extragalactic fields. While a certain correlation between H $\alpha$  and [O III] is expected for star forming galaxies, such a log-linear and tight (dispersion of  $\sim 0.1$  dex) and trend is hard to explain because dust reddening would skew any intrinsic relation between the two. Furthermore, another surprising finding emerges from investigating the dust reddening properties of these galaxies. We find that the classic method of using the Balmer decrements under the standard Case B assumption does not work: a high fraction ( $\sim 40\%$ ) of our objects have H $\alpha$ /H $\beta$  line ratios even smaller than the canonical Case B ratio of 2.86. Such a high fraction of non-Case B Balmer decrements is also present in other JWST and ground-based spectroscopic studies, but the universal applicability of the Case B assumption was not questioned until recently. The mysterious H $\alpha$ -[O III] correlation and the high fraction of non-Case B Balmer decrements, which may or may not be related, should be further investigated to put our spectral analysis onto a more solid footing.

## 1. INTRODUCTION

Emission line diagnostics is a fundamental tool in studying the physical properties of star-forming galaxies, which can provide deep insights into their star formation rates (SFRs), chemical compositions, evolutionary histories, etc. (e.g., [L. J. Kewley et al. 2019](#)). Two emission lines, H $\alpha$  $\lambda$ 6563 and [O III] $\lambda$  $\lambda$ 4959, 5007 doublet, are the most studied ones because they are usually the strongest lines among all. The H $\alpha$  line is widely adopted as a robust tracer of instantaneous SFR because its intensity is directly related to the ionizing radiation from young, high-mass stars ([R. C. Kennicutt 1998](#)). The [O III] doublet, on the other hand, is often used as a probe of the ISM ionization state (e.g., [J. A. Baldwin et al. 1981](#); [L. J. Kewley & M. A. Dopita 2002](#); [R. Maiolino et al. 2008](#)).

The utilization of these two lines in large samples used to be confined to  $z < 4$  due to the limitation of the instrumental capabilities. As an example, the Keck MOSDEF spectrograph cuts off at  $2.4 \mu\text{m}$ , which can only detect H $\alpha$  and [O III] up to  $z \approx 2.7$  and  $z \approx 3.8$ , respectively. The advent of the James Webb Space Telescope (JWST) has greatly expanded our ability in this regard. In particular, its NIRSpec instrument has been routinely discovering H $\alpha$  emitters up to  $z \approx 6$  and [O III] emitters up to  $z \approx 9$ . Moreover, its unprecedented sensitivity now allows studies in the regime more than an order of magnitude fainter than previously probed. Over more

than two years of science operation, JWST has accumulated a sufficiently rich spectroscopic dataset that is public to all to explore the uncharted territory.

To this end, we started an investigation on H $\alpha$  and [O III] emission lines using the public archival JWST NIRSpec data, with the simple motivation of re-examining the correlation between the two. Past studies have explored the use of [O III] as a proxy to H $\alpha$  and thus a tracer for SFRs, especially at higher redshifts where H $\alpha$  becomes inaccessible (e.g., the study of [T. L. Suzuki et al. 2016](#) at  $z = 2.23$ ). [J. A. Villa-Vélez et al. \(2021\)](#) found a linear relation between [O III] luminosity and SFR at  $z \approx 1.6$ , although the relation shows large scatters due to variations in factors such as metallicity. [R. Wen et al. \(2022\)](#) found that [O III] emission could trace star formation in dusty galaxies at  $z = 3.25$  with proper calibrations. In contrast, studies like [J. Moustakas et al. \(2006\)](#) and [M. Figueira et al. \(2022\)](#) noticed that without accounting for different metallicities and ionization states, using the [O III] line alone might not yield reliable SFR estimates. Despite these tentative results, no comprehensive studies have been done to investigate the correlations between H $\alpha$  and [O III] over a wide redshift range or below the limit of  $\sim 10^{-17} \text{ erg s}^{-1} \text{ cm}^{-2}$ , and we aimed to start filling the blank.

Using both the low-resolution ( $R \sim 100$ ) and the mid-resolution ( $R \sim 1000$ ) spectra taken by the NIRSpec instrument, we carefully constructed a large sample where

the  $H\alpha$  and [O III] lines could be measured reliably. To our surprise, our initial study revealed a very tight, linear correlation between the  $H\alpha$  and [O III] line fluxes in the logarithmic space *before* applying any dust reddening correction. While at the first glance it seems to be encouraging in that [O III] could be as good as  $H\alpha$  in tracing SFRs, this correlation is in fact problematic because dust reddening should destroy any intrinsic correlation between these two lines. In other words, the *observed* correlation should not have such a linear and tight behavior with the presence of dust. Therefore, we went on to check the dust reddening properties of these galaxies using the Balmer decrement method, which has long been regarded as the most reliable method of deriving dust extinction (e.g., D. Calzetti et al. 1994). To our surprise again, we found that  $\sim 40\%$  of our objects have  $H\alpha/H\beta$  line ratio less than the dust-free Case B value of 2.86. This is a more severe problem, because the Case B recombination is the underlying assumption of the Balmer decrement method; if the Case B assumption fails, the Balmer decrement method also fails in measuring dust extinction. As it turns out, non-Case B Balmer decrements have been reported sporadically in the literature, however, the universality of the Case B assumption was not questioned until recently (N. Pirzkal et al. 2024; C. Scarlata et al. 2024).

While it is unclear whether they are related, these two findings are important enough for us to call for further investigations to understand their physical mechanisms. In this paper, we present them in detail. We describe the spectroscopic data in Section 2, including the line measurements and the sample construction. Section 3 shows our key findings, and Section 4 discusses the implications. We summarize and conclude this work in Section 5.

## 2. JWST NIRSPEC SPECTROSCOPY DATA

### 2.1. Data Reduction

We mainly used the public NIRSpec MSA data taken in the GOODS-S, GOODS-N, and EGS fields for this study. These data are from the JWST Advanced Deep Extragalactic Survey (JADES; D. J. Eisenstein et al. 2023) in the two GOODS fields (PIDs 1180, 1181, 1210, 1286, 3215; see also F. D’Eugenio et al. 2024), and the Cosmic Evolution Early Release Science Survey (CEERS; S. L. Finkelstein et al. 2025) in the EGS field (PID 1345; see also P. Arrabal Haro et al. 2023). These observations were all done in a 3-shutter-nod configuration. The JADES data were taken in four disperser/filter setups: PRISM/CLEAR, G140M/F070LP, G235M/F170LP, and G395M/F290LP. The CEERS data were taken using similar setups, with the only difference that the filter used for G140M was F100LP. Hereafter, we denote the PRISM/CLEAR setup as “PRISM” and the other three grating setups as “Grating”, respectively. Under the PRISM setup, the nominal resolving power is  $R \sim 100$  and the spectral cov-

erage is  $0.6\text{--}5.3 \mu\text{m}$ . The spectral resolution for all medium-resolution grating setups (G140M, G235M, and G395M) is  $R \sim 1000$ , and the wavelength ranges are  $0.70\text{--}1.27/0.97\text{--}1.84$  (with F070LP/F100LP),  $1.66\text{--}3.07$ , and  $2.87\text{--}5.10 \mu\text{m}$ , respectively.

In this work, we reduced these data on our own. We started from the Level 1b products retrieved from the Mikulski Archive for Space Telescopes (MAST). We first processed them through the `calwebb_detector1` step of the standard JWST pipeline (version 1.16.0; H. Bushouse et al. 2024) in the context of `jwst_1312.pmap`. We then processed the output “rate.fits” files through the MSAEXP package (version 0.9.2; G. Brammer 2023), which provides an end-to-end reduction from the “rate.fits” to the final spectra extraction. The procedure removes the “1/f” noise pattern, the “snowball” defects, subtracts the bias level, does flat-fielding, applies path-loss correction and flux calibration, and traces spectra on all single exposures; lastly, it combines all single exposures with outlier rejection. The background subtraction is done using the measurement in the nearest blank slit.

For an object that has grating spectra taken in different disperser/filter setups, we further combined them into one single spectrum. This was done by first constructing a common wavelength grid that spans from the shortest to the longest wavelength in the individual grating spectrum. The wavelength arrays were then combined, and the grid adopted the sampling from the longer-wavelength grating in the overlapping regions. Then, each grating spectrum was resampled onto this common wavelength grid using linear interpolation. In regions where the spectra overlap, the flux values were combined using a weighted average based on the inverse square of their errors.

### 2.2. Sample Selection and Line Flux Measurements

From the reduced data, we selected the spectra that have both  $H\alpha$  and [O III] detections. We further imposed an additional selection based on the continuum fitting. Specifically, we performed continuum fitting on all available spectra using high-order polynomials (detailed below) and retained only those that yielded robust continuum fits. This stringent selection minimizes the systematic uncertainties due to poor continuum subtraction and therefore further ensures the reliability of our line flux measurements. In total, 563 spectra were selected. Among these, 251 are PRISM spectra and 312 are Grating spectra, with 83 galaxies in common. The total number of unique galaxies is 480. They span a wide redshift range of  $z \approx 1.5\text{--}7$ , which is shown in Figure 1. We detail our sample selection process and line flux measurements below.

#### 2.2.1. Low-resolution PRISM Spectra

We fitted the continua of the PRISM spectra with a seventh-order Chebyshev polynomial us-

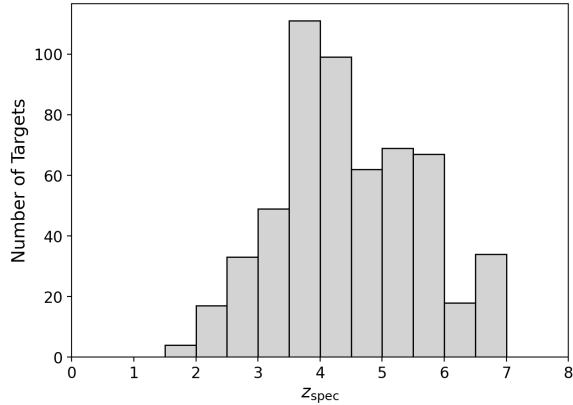


**Figure 1.** Redshift distribution of the 480 unique galaxies in our sample, combining both the PRISM and the Grating sets.

ing the `fit_generic_continuum` function in the `ASTROPY/SPECUTILS` package (N. Earl et al. 2024). The fit was done after excluding the regions  $0.1 \mu\text{m}$  centering all strong emission lines. In a few cases where a seventh-order polynomial did not fit well, we used higher-order polynomials up to the tenth order. After subtracting the fitted continua from the spectra, we fitted Gaussian profiles to the targeted lines. The line fluxes were measured within  $2 \times \text{FWHM}$  from the central wavelengths. Most of the lines (e.g.  $\text{H}\alpha$ ) were fitted using a single Gaussian profile. For the  $[\text{O III}]\lambda\lambda 4959, 5007$  doublets, a double-Gaussian profile was used. Some lines of different species are severely blended, and we found that there must be at least three wavelength bins between the line centers in order to reliably separate them. As a result, we had to exclude the objects at  $z < 2.3$  because of the severe blending of  $\text{H}\beta$  and  $[\text{O III}]\lambda 4959$  due to the poor spectral resolution at  $\lambda < 1.65 \mu\text{m}$ . In the end, we selected 251 PRISM spectra that have both  $\text{H}\alpha$  and  $[\text{O III}]\lambda\lambda 4959, 5007$  emission lines detected at  $\text{S/N} \geq 3$ . We note that the line flux and the  $\text{S/N}$  of the  $[\text{O III}]$  doublet is calculated by combining its two lines. We also note that we excluded any objects that have a broad component in the Balmer lines, which indicates the presence of an AGN.

Two objects from the PRISM sample are shown in Figure 2 as examples. The top panel shows a galaxy at  $z = 3.6$  with a blended  $[\text{O III}]$  doublet that cannot be separated individually. As mentioned above, we fitted a double-Gaussian profile to the doublet to measure them as a whole. The nearby  $\text{H}\beta$  line is shifted to  $\lambda_{\text{obs}} \approx 2.25 \mu\text{m}$ , which is sufficiently separated from the  $[\text{O III}]$  doublet so that the fitting procedure could exclude  $\text{H}\beta$  and provide reliable measurement of the  $[\text{O III}]$  doublet. The middle panel shows a galaxy at  $z = 5.9$ , which has the  $[\text{O III}]$  doublet resolved with two clear peaks. In this case, the double-Gaussian profile would separate the doublet.

### 2.2.2. Medium-resolution Grating Spectra

The flux measurements and the sample selection using the grating spectra were done similarly to the above, with a few changes: (1) the continuum shapes were less complex in the grating spectra, and therefore we used a fifth-order polynomial instead; (2) all lines were fitted using a single-Gaussian profile, as the lines are well separated; (3) the  $z \geq 2.3$  limit was lifted because the spectral resolution is high enough to separate  $\text{H}\beta$  from  $[\text{O III}]$  at any redshifts. In the end, we selected 312 grating spectra independent of the PRISM sample. The bottom panel of Figure 2 shows one example.

### 2.3. Subsample for Balmer Decrement Measurement

The “gold standard” of deriving dust reddening of galaxies is to use the Balmer decrement, most commonly the ratio between  $\text{H}\alpha$  and  $\text{H}\beta$ , under the Case B assumption of the hydrogen recombination. A fraction of our objects have strong enough  $\text{H}\beta$  line allowing us to carry out this practice, for which we selected a subsample where the  $\text{H}\beta$  line detections have  $\text{S/N} \geq 3$ . This subsample consists of 179 PRISM and 265 grating spectra, with 66 in common.

In what follows, we will derive the gas-phase dust reddening by following the extinction law of D. Calzetti et al. (2000):

$$E(B - V)_{\text{gas}} = \frac{\log_{10}(R_{\text{obs}}/R_{\text{int}})}{0.4(k_{\text{H}\beta} - k_{\text{H}\alpha})}, \quad (1)$$

where  $k_{\text{H}\alpha} = 3.327$  and  $k_{\text{H}\beta} = 4.598$ .  $R_{\text{obs}}$  is the observed line flux ratio between  $\text{H}\alpha$  and  $\text{H}\beta$ , and  $R_{\text{int}} = 2.86$  is the widely adopted intrinsic ratio in the Case B recombination at an electron temperature of  $T_e = 10^4 \text{ K}$  and an electron density of  $n_e = 10^2 \text{ cm}^{-3}$  (D. E. Osterbrock 1989).

### 2.4. Consistency Check of Line Measurements in PRISM and Grating Sets

To ensure that we can use a combined sample of the PRISM and the Grating sets, we conducted a consistency check of the line flux measurements on  $\text{H}\alpha$ ,  $[\text{O III}]$ , and  $\text{H}\beta$  emission lines using the common objects in these two sets. This check is presented in Figure 3.

While the fluxes generally agree well, there are disagreements present. Especially for  $\text{H}\alpha$ , there are cases where the flux measurements from PRISM spectra are significantly stronger. A major reason for such disagreements is due to the low resolution of PRISM spectra, which may cause the blending of the nearby  $[\text{N II}]$  lines and therefore resulting in an overestimate of the  $\text{H}\alpha$  flux. Fortunately,  $[\text{N II}]$  contributes insignificantly in most cases. Other factors, such as background subtraction and continuum subtraction, may also lead to those outliers since line flux measurements are very sensitive to such effects.

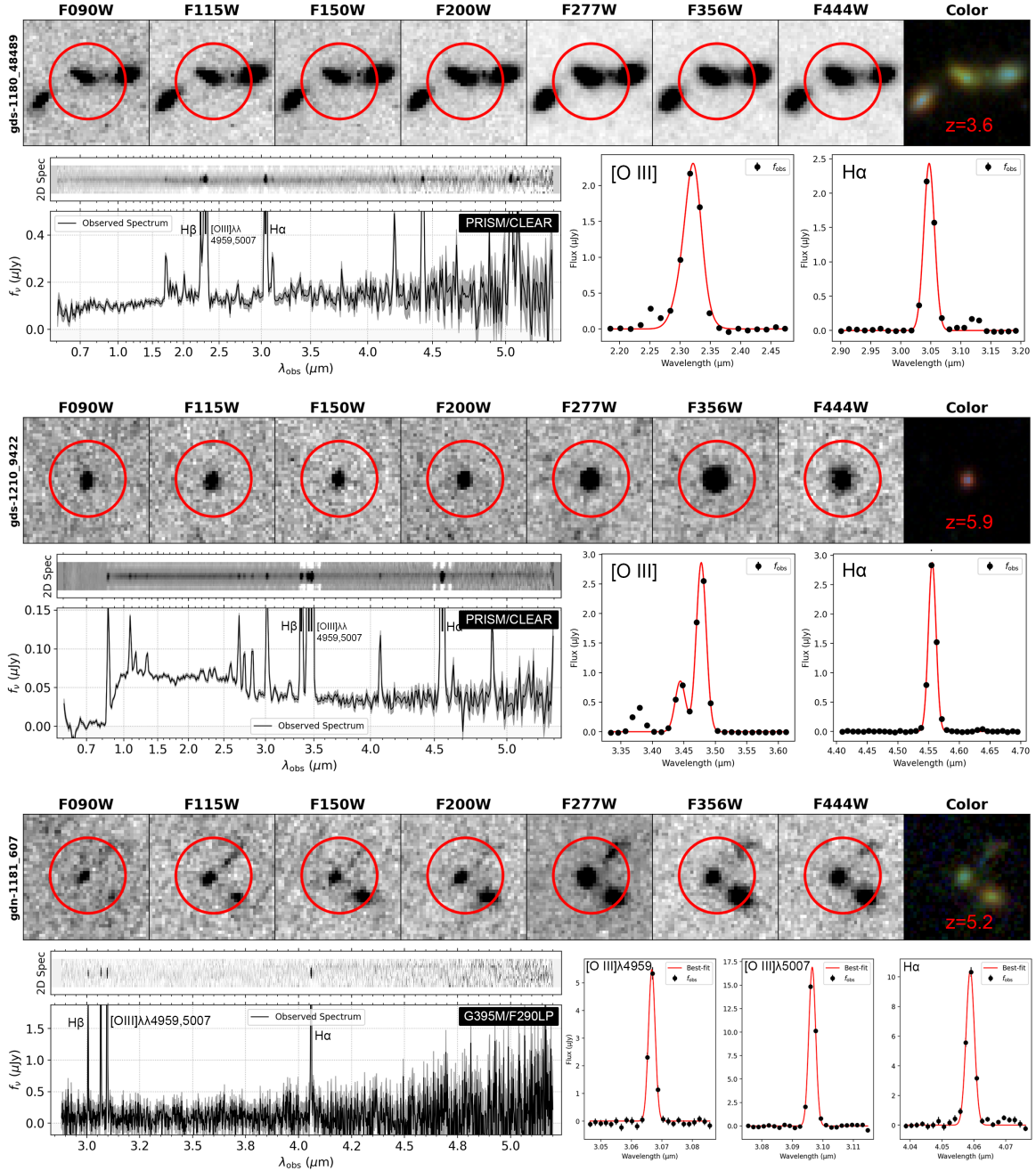


**Figure 2.** Example PRISM and medium-resolution grating spectra. *Upper panel:* an object at  $z \approx 3.6$  whose [O III] doublet is unresolved in PRISM spectrum; *Middle panel:* another PRISM spectrum but the [O III] doublet is clearly resolved into two peaks; *Lower panel:* an example showing individual emission line fits using the grating spectrum, specifically, G395M in this case.

Despite these disagreements, the tight agreement to the 1:1 lines indicates that systematic differences between PRISM and Grating spectra do not significantly impact our analysis on the combined sample.

### 3. RESULTS

#### 3.1. Tight Correlation between $H\alpha$ and [O III]

The left panel of Figure 4 shows the relation between the  $H\alpha$  and the [O III] doublet line fluxes in logarithm, using both the PRISM sample (black symbols) and the Grating sample (red symbols). Surprisingly, the relation is an extremely tight linear correlation. We fitted

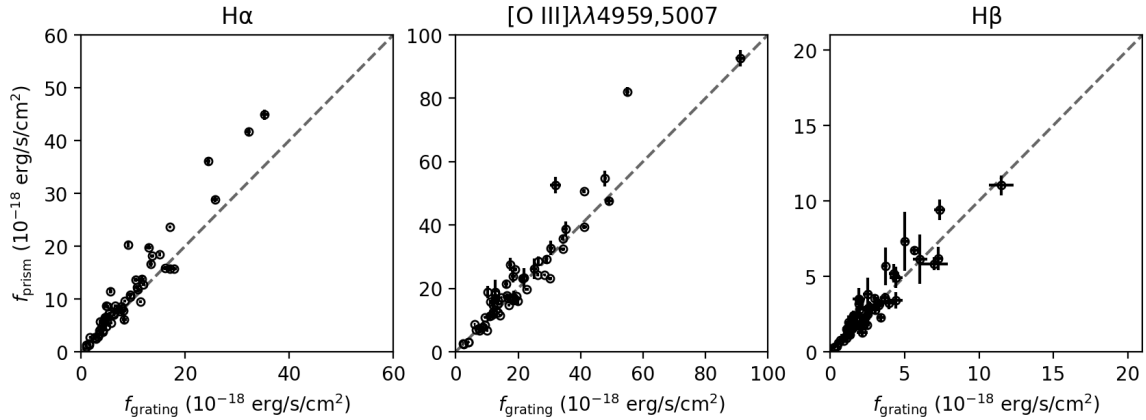


**Figure 3.** Comparison of line fluxes for H $\alpha$  (left), [O III] (center), and H $\beta$  (right) measured from PRISM and Grating spectra for the common objects. The X-axis represents the flux measurements from the Grating set ( $f_{\text{grating}}$ ) and the Y-axis represents those from PRISM set ( $f_{\text{prism}}$ ), both in the unit of  $10^{-18}$  erg/s/cm $^2$ . A straight line is plotted to indicate 1:1 agreement between the two measurements.

a simple linear function in the form of

$$\log_{10}(f_{\text{H}\alpha}) = k \times \log_{10}(f_{\text{[O III]}}) - b \quad (2)$$

and obtained the best-fit coefficients  $(k, b) = (1.03 \pm 0.03, -0.41 \pm 0.04)$ , with the root mean square (rms) value of only 0.104. This linear form is shown as the solid black line in the figure, with the gray-shaded regions indicating the  $2\sigma$  error range. Separating the PRISM and the Grating samples does not make any notable difference in the fitted relation.

Such a tight linear correlation is unexpected, as not all the galaxies can be dust-free and therefore statistically the [O III] line must suffer more severe extinction than the H $\alpha$  line does. To verify whether this could be due to our sample being somewhat biased because of our stringent requirement in the continuum fitting, we checked for the correlation using the results from two other teams, namely, the spectroscopic catalogs from the public releases of the JADES DR3 (F. D’Eugenio et al. 2024) and the DR4 of the Ultradeep NIRSpec and NIRCам Observations before the Epoch of Reionization program (UNCOVER; R. Bezanson et al. 2024; S. H. Price et al. 2024). Both catalogs are based on the PRISM spectra. We only used the objects with reliable spectroscopic redshifts  $z_{\text{spec}}$  from these catalogs (ranks A, B, C in JADES DR3; ranks 2, 3 in UNCOVER) and only retained those that have  $\text{S/N} \geq 3$  line fluxes in H $\alpha$  and [O III] to be consistent with our sample selection. In total, there were 1128 and 164 spectra from JADES and UNCOVER used in the comparison, respectively. The correlation between H $\alpha$  and [O III] from these independent measurements of two different teams is the same as ours, and the comparison is shown in the right panel of Figure 4. There are 428 objects in common between our sample and the JADES sample. Had there been any systematic differences between these two sets, one would observe some offsets

for these common objects in this comparison. However, no such offsets are seen. Therefore, we conclude that our sample is not biased, nor are our line measurements erroneous. Fitting the same linear relation with all three datasets combined (ours + JADES + UNCOVER), we got  $(k, b) = (1.05 \pm 0.02, -0.37 \pm 0.01)$  and RMS value of 0.160; in other words, both the slope and intercept are only marginally different from what we obtained using only our sample. When fitting the same relation with JADES and UNCOVER alone, we got  $(k, b) = (1.07 \pm 0.02, -0.43 \pm 0.02)$  and  $(1.10 \pm 0.04, -0.41 \pm 0.06)$ , and RMS values of 0.150 and 0.143, respectively.

To investigate the possible redshift dependency of the correlation, we divided the spectra into four redshift bins:  $1.5 \leq z < 2.5$ ,  $2.5 \leq z < 4$ ,  $4 \leq z < 6$ , and  $z \geq 6$ . Figure 4 show the H $\alpha$ -[O III] relation in these four bins using our sample alone (middle row) and when combining all the three samples (bottom row). In all four redshift bins, the Pearson correlation coefficient consistently remains  $R > 0.8$ , and notably, the correlation appears to be even tighter at higher redshifts. We fitted the same linear relation in these four ranges, and the best-fits to our sample have  $(k, b) = (0.90 \pm 0.09, -0.21 \pm 0.16)$ ,  $(1.06 \pm 0.02, -0.49 \pm 0.04)$ ,  $(0.97 \pm 0.02, -0.39 \pm 0.02)$ , and  $(0.96 \pm 0.04, -0.36 \pm 0.05)$ , respectively; and those to three datasets combined are  $(k, b) = (1.11 \pm 0.02, -0.36 \pm 0.02)$ ,  $(1.02 \pm 0.02, -0.37 \pm 0.02)$ ,  $(0.95 \pm 0.02, -0.34 \pm 0.03)$ ,  $(0.97 \pm 0.03, -0.40 \pm 0.03)$ . While these values seem to suggest a slight decrease in the slope at higher redshifts, the differences are not statistically significant. If there is any redshift-dependent trend, it is that the relation seems to be tighter at higher redshifts.

### 3.2. Comparing to the pre-JWST results

Surprised by the tight correlation discussed above, we checked the published results from a few large spectro-

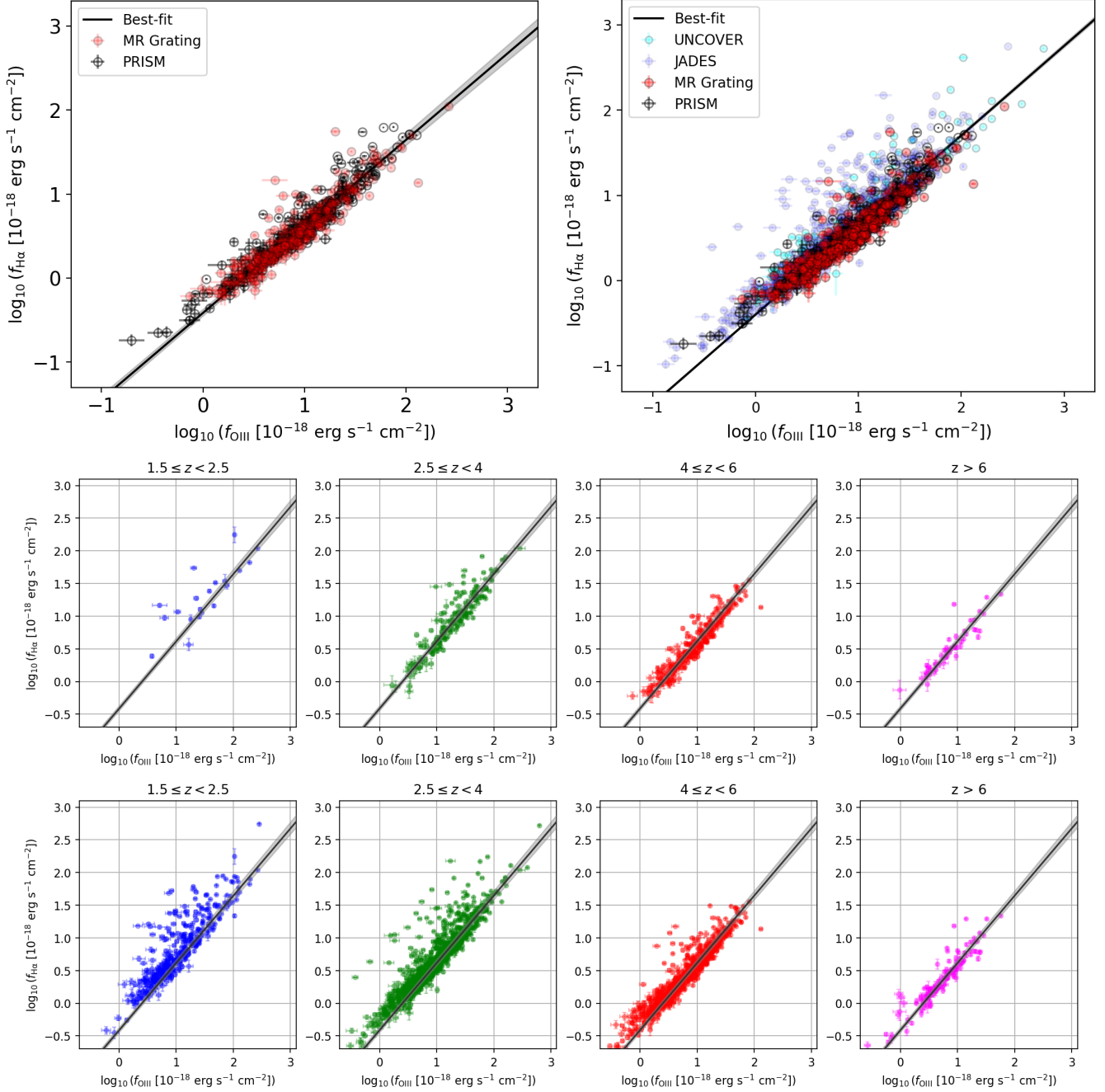


**Figure 4.** *Top panels:* Tight linear relation between H $\alpha$  and [O III] line fluxes in logarithm as revealed by our sample (left) and also seen in the NIRSPEC catalogs released by the JADES and the UNCOVER teams (right). The straight line in the left panel is the best-fit to the combined PRISM and Grating sets, while the one in the right panel is the best-fit to our sample plus the ones from the JADES and the UNCOVER catalogs. The  $2\sigma$  uncertainty is indicated by the gray areas. *Middle panels:* Similar to the top-left panel (i.e., using only the data from our sample) but to show the H $\alpha$ –[O III] correlation in four successive redshift bins. *Bottom panels:* Similar to the middle panels but using data combining our sample and those from JADES and UNCOVER programs.

scopic surveys in the pre-JWST era. As it turns out, such a correlation is also present in these data, albeit with much larger dispersions. Here we highlight the comparison with the measurements from the MOSFIRE Deep Evolution Field program (MOSDEF; M. Kriek et al. 2015) and the ZFIRE program (T. Nanayakkara et al. 2016) carried out by the MOSFIRE instrument at the Keck-1 telescope and the FMOS-COSMOS program (D. Kashino et al. 2019) done by the FMOS spectrograph at the Subaru telescope. These three programs spanned the redshift range of  $z \sim 1\text{--}2.5$ , for which we can make a direct comparison. This is demonstrated in Figure 5, where the NIRSspec data points in this range are shown in blue and those from the three ground-based programs are shown in magenta. The latter also follows a linear trend with  $(k, b) = (0.80 \pm 0.06, 0.32 \pm 0.15)$ , but the distribution lies slightly above our relation and has a much larger dispersion (RMS of 0.403).

We also checked the line flux measurements from the Sloan Digital Sky Survey (SDSS) value-added MPA-JHU catalog <sup>2</sup> for the situation at  $z < 1$ . The correlation is no longer obvious in these data. As currently there are insufficient number of NIRSspec measurements at  $z < 1$ , we do not make a direct comparison here.

### 3.3. Conflict with Dust Reddening

The very tight, linear correlation between  $\log_{10}(\text{H}\alpha)$  and  $\log_{10}([\text{O III}])$  seen in the NIRSspec spectra suggests that there is an intrinsic, fixed ratio between the two lines. However, even if such a fixed ratio exists, the observed ratios would deviate from this value because of the dust reddening. In other words, such a relation would only make sense if, for some reason, the target selections for NIRSspec spectroscopy by these programs were all biased in favor of dust-free galaxies. However, this does not seem to be the case.

Our subsample for the Balmer decrement measurement allows us to derive the gas-phase dust reddening  $E(B - V)_{\text{gas}}$  for these objects (see Section 2.3). Under the standard Case B assumption, most of them have significant reddening, which is inconsistent with the linear relation between  $\log_{10}(\text{H}\alpha)$  and  $\log_{10}([\text{O III}])$ : if the intrinsic relation between the two is indeed linear, dust reddening would suppress  $[\text{O III}]$  more than  $\text{H}\alpha$ , which would then skew the linear relation. Or in other words, the dust reddening and the intrinsic line ratio would have to conspire in a delicate way such that the observed relation is linear. This point is demonstrated in the top-left panel of Figure 6 in the form of flux ratio of  $\text{H}\alpha$  and  $[\text{O III}]$  versus  $E(B - V)_{\text{gas}}$ . As  $k$  in Equation 2 is very close to unity, the line ratio represents well the observed log-linear relation. The data points concentrate at the value of  $f_{\text{H}\alpha}/f_{[\text{O III}]} \approx 0.4$ , which is the manifest of the best-fit intercept of  $-0.41$  that we

obtained ( $10^{-0.41} \approx 0.39$ ) in Figure 4. If there is an intrinsic, fixed ratio between the two lines, the observed line ratio should be changed by the dust reddening. This is indicated by the yellow dashed curve, which is the predicted behavior of the observed line ratio due to reddening when assuming an intrinsic ratio of 0.4. The top-right panel shows the multiplicative factor that needs to be applied to move the data points to the yellow dashed curve, which are effectively the ratios of the observed and the predicted  $f(\text{H}\alpha)/f([\text{O III}])$ .

### 3.4. Non-Case B $\text{H}\alpha/\text{H}\beta$ Ratios

A more severe problem is revealed while investigating the dust reddening. As shown in these two panels, there are a large number of objects that have negative  $E(B - V)$  values (see the grey area), which is unphysical. We find that this is due to fact that a large number of our objects have  $f_{\text{H}\alpha}/f_{\text{H}\beta}$  values smaller than the canonical Case B value of 2.86. The fraction is  $\sim 30\%$  and  $\sim 50\%$  in the PRISM set and the Grating set, respectively. Being surprised, we check this line ratio in the JADES and the UNCOVER catalogs as well as in the three ground-based redshift survey catalogs discussed in Section 3.2. As it turns out, all these catalogs have a large fraction of objects ( $\sim 30\%$  in JADES and UNCOVER and also  $\sim 30\%$  in MOSFIRE+FMOS) that have  $f_{\text{H}\alpha}/f_{\text{H}\beta} < 2.86$ , which is shown in the histograms in Figure 6. This is a strong indication that the Case B assumption is not universally applicable, which we will discuss in the next section.

## 4. DISCUSSION

### 4.1. Comparison of Dust Extinction Derived from Two Methods

To further investigate the dust reddening problem, we used a different approach. For all the galaxies in our subsample for measuring the Balmer decrements, we derived their dust extinction  $A_V^s$  by fitting their spectral energy distributions (SEDs), which can then be compared to the gas-phase dust extinction  $A_V^g$  based on the Balmer decrements discussed above. Note that  $A_V^s$  is the extinction of stellar light and is different from the gas-phase extinction; adopting the Calzetti's extinction law implies that  $A_V \approx 4.04 \times E(B - V)$  and  $E(B - V)_{\text{star}} = 0.44 \times E(B - V)_{\text{gas}}$ .

The SEDs of all our objects were constructed using the PSF-matched photometry of B. Sun & H. Yan (2025). To fit the SEDs, we used BAGPIPES (A. C. Carnall et al. 2018, version 1.2.0), which utilizes the stellar population synthesis models of G. Bruzual & S. Charlot (2003) with the initial mass function of P. Kroupa (2001). We ran the program using the delayed- $\tau$  star formation history, which is in the form of  $\text{SFR} \propto te^{(-t/\tau)}$ . We set  $\tau$  as a free parameter that could vary between 0.01–15 Gyr. The metallicity was also set free in the range of  $0 \leq Z/Z_{\odot} \leq 2.5$ , and the dust extinction  $A_V$  could vary from 0 to 8 mag. We also enabled the option to include nebular emission lines, and the ionization parameter could vary

<sup>2</sup> <https://wwwmpa.mpa-garching.mpg.de/SDSS/DR7/>

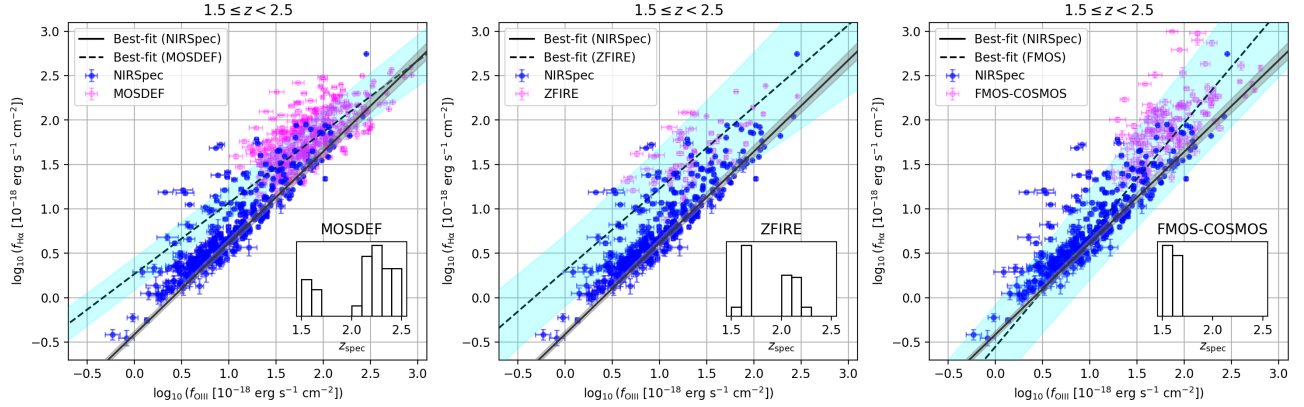


**Figure 5.** Comparison of the  $H\alpha$ –[O III] relation obtained with NIRSpect (combining our sample, JADES and UNCOVER; blue symbols) and that from the three ground-based surveys (magenta symbols) using Keck/MOSFIRE (the MOSDEF and zFIRE programs) and Subaru/FMOS (the FMOS-COSMOS program) in our lowest redshift bin of  $1.5 \leq z < 2.5$ . The solid black straight line and the gray areas indicate the same linear correlation and the dispersion as in the lower-left panel of Figure 4, while the dashed straight line and the cyan areas indicate the best linear fit to the three ground-based survey data and the dispersion. The insets show the redshift distributions of the three ground-based samples.

between  $-4.0 \leq \log(U) \leq -2.0$ . The redshift of each target is fixed at its  $z_{\text{spec}}$ .

For clarity, we denote the  $A_V^S$  values derived from the SED fitting above as  $A_V(\text{SED})$  and the  $A_V^S$  values converted from  $E(B - V)_{\text{gas}}$  based on the Balmer decrement measurements as  $A_V(\text{BD})$ . The comparison of the two is presented in Figure 7. Simply put, the two do not agree, and  $A_V(\text{SED})$  is larger than  $A_V(\text{BD})$  in most cases. To some extent, the disagreement could still be explained if the star-forming regions that give rise to the nebular emission lines are not well mixed with the rest of the stellar populations. However, it is more likely that this is another indication of the failure of measuring dust extinction using the Balmer decrement. In particular, those with unphysical  $A_V(\text{BD}) < 0$  still have significant  $A_V(\text{SED})$ .

#### 4.2. Non-Case B Recombination

All our analysis above suggests that the usual practice of deriving dust extinction through the Balmer decrement can be problematic. The strongest indication comes from the high fraction of galaxies that have  $H\alpha$  and  $H\beta$  line ratios that are smaller than the dust-free Case B value. Such objects are present in both our PRISM and Grating sets and therefore cannot be attributed to different spectral resolutions of the data. They are also found in high fractions in at least two public NIRSpect catalogs from two independent teams and therefore are not likely due to measurement flaws. Moreover, they also exist in similarly high fractions in three ground-based redshift survey programs in the pre-JWST era, which means that it is a universal problem already observed but largely unexplored. In fact, the SDSS value-added MPA-JHU catalog also contains such objects at a low but non-negligible fraction ( $\sim 6\%$ ), however this was not discussed in the literature until recently

(see C. Scarlata et al. 2024). There have been a few studies that noticed such anomalies but did not discuss them in the context of non-Case B possibility, which we summarize in Appendix.

The universality of the Case B assumption was recently questioned by N. Pirzkal et al. (2024), who analyzed the grism slitless spectroscopic data ( $R \sim 150$ ) taken by the JWST NIRISS instrument in the historic Hubble Ultra Deep Field. Among their 91 galaxies at  $1 < z < 3.5$  whose  $H\alpha$  and  $H\beta$  lines are detected at  $S/N > 2$ , 30% have the  $H\alpha/H\beta$  line ratios smaller than 2.86. C. Scarlata et al. (2024) also challenged the Case B assumption using a single galaxy at  $z = 0.0695$ , for which they measured the  $H\alpha/H\beta$  ratio of 2.62 based on the  $R \sim 867$  spectrum taken at the MMT. By considering other line ratios, they suggested that the deviation is likely driven by physical mechanisms, most likely the Balmer self-absorption and scattering effects in non-spherically symmetric gas geometries.

Our result enhances the argument that the Case B recombination is not universally applicable. As compared to the study of N. Pirzkal et al. (2024), our result is drawn from a much enlarged sample (by  $> 4\times$ ) over a much wider redshift range ( $1.5 \leq z \leq 7$ ), and our line measurement, thanks to the NIRSpect MSA mode, is not prone to the data reduction complications that slitless spectroscopy usually suffers. In other words, there is now sufficient evidence that the Case B assumption does not universally hold, at least not in the redshift range that our sample probes.

We note that the failure of the Case B assumption is not necessarily only limited to the galaxies that have  $H\alpha/H\beta$  ratios less than 2.86, which is also a point raised in N. Pirzkal et al. (2024) and C. Scarlata et al. (2024). For example, galaxies with intrinsic non-Case B Balmer decrements could have dust reddening that easily creates



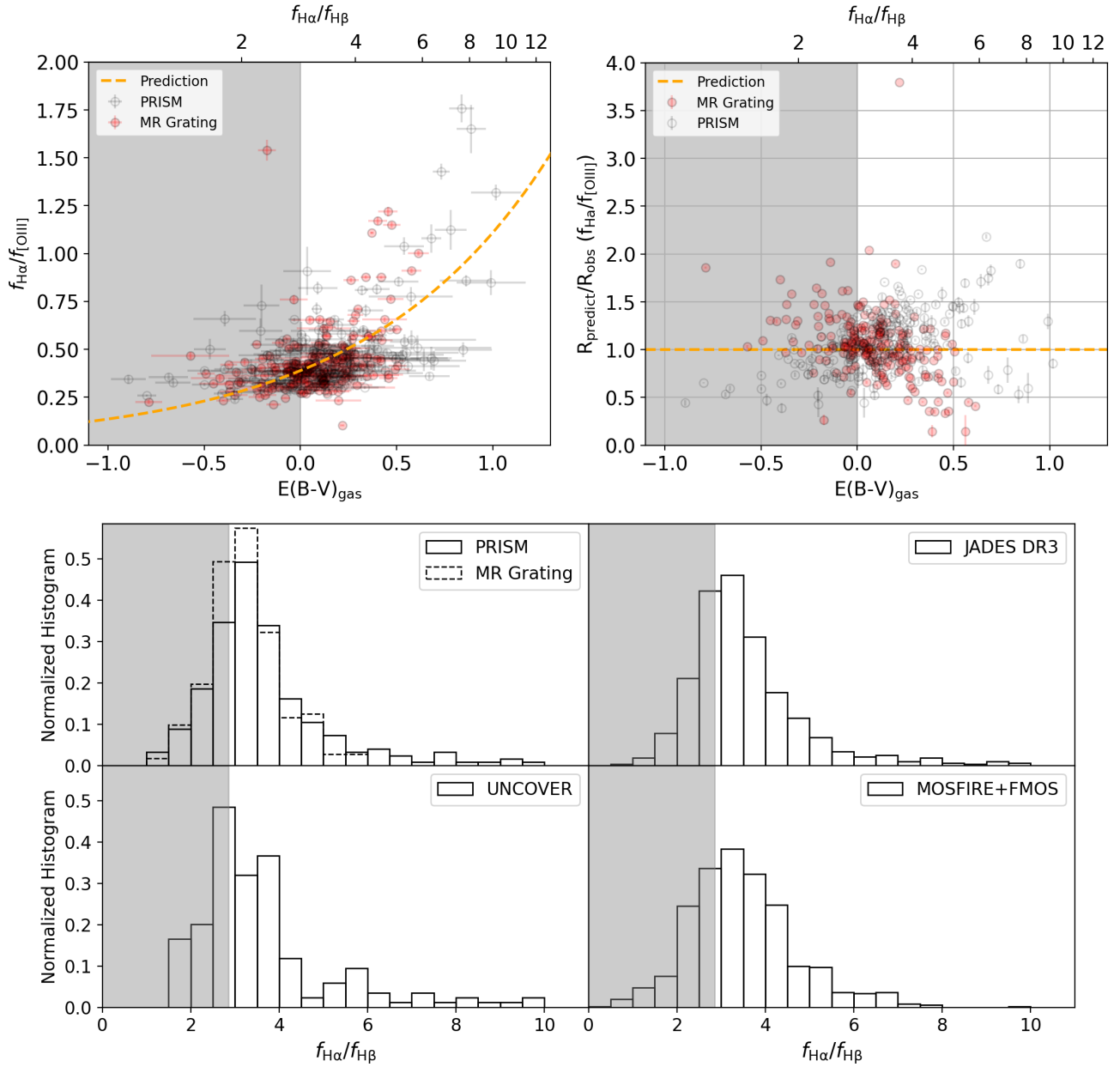


**Figure 6.** *Top-left:* Relations between the  $\text{H}\alpha/[\text{O III}]$  flux ratios and the estimated gas-phase dust reddening  $E(\text{B} - \text{V})_{\text{gas}}$  under the Case B assumption and the Calzetti’s extinction law. The PRISM and the Grating data from our sample are shown as the gray and the red symbols, respectively. The dashed orange curve is the predicted behavior of  $\text{H}\alpha/[\text{O III}]$  as a function of  $E(\text{B} - \text{V})_{\text{gas}}$ . The gray-out area is where  $E(\text{B} - \text{V})_{\text{gas}} < 0$  due to the non-Case B ratios (see the bottom panels). *Top-right:* Multiplicative factors that need to be applied to the observed  $\text{H}\alpha/[\text{O III}]$  ratios to move them to the predicted behavior as shown in the left panel. *Bottom:* Histogram of  $\text{H}\alpha/\text{H}\beta$  line ratios from our sample, from two other public catalogs using JWST NIRSpec (JADES and UNCOVER) and from three ground-based programs (MOSDEF, zFIRE, and FMOS-COSMOS), respectively. The line ratios smaller than the canonical Case B values of 2.86 (indicated by the gray-out area) are present in high fraction ( $\sim 40\%$  in our sample and  $\sim 30\%$  in others) in all these samples, suggesting the Case B assumption is not universally applicable.

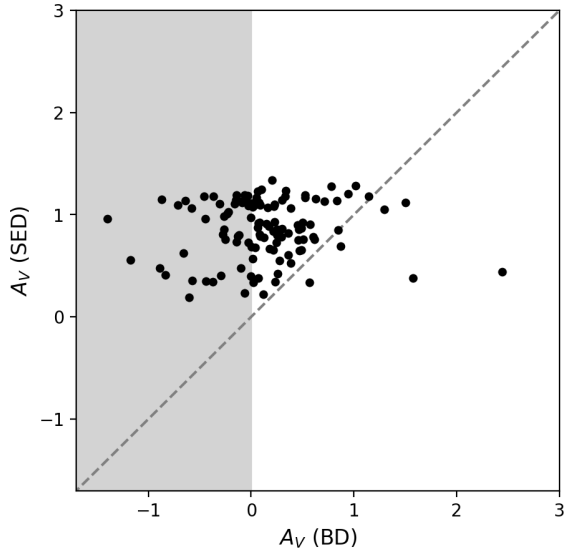


**Figure 7.** Comparison between dust extinction  $A_V$  derived from the SED fitting (denoted as  $A_V(\text{SED})$ ) and converted from the gas-phase extinction based on the Balmer decrement (denoted as  $A_V(\text{BD})$ ). The dashed black line shows the 1:1 correspondence. The grey-out area is where the objects have  $A_V(\text{BD}) < 0$  due to their  $\text{H}\alpha/\text{H}\beta$  line ratio being lower than the canonical Case B value of 2.86. There is hardly any trend between the two, which further enhances the argument that the Case B assumption is not universally applicable.

line ratios that do not seemingly violate the Case B limit and therefore are disguised. Our community will need to re-think how to assess dust reddening/extinction in extragalactic studies in general.

#### 4.3. Mysterious $\text{H}\alpha$ -[O III] Correlation

The mysteriously tight correlation between  $\text{H}\alpha$  and [O III] is what we observe *before* applying any dust extinction correction, and therefore is independent of the non-Case B recombination problem discussed above. Based on the SED fitting, most of these objects have non-negligible dust reddening, and therefore the linearity observed can hardly be explained. As shown in Figure 4, the relation remains tight in four successive redshift bins, and there is no obvious redshift evolution from  $z \approx 2$  to  $z \approx 7$ . In contrast, the results from the three ground-based redshift surveys that we examined do not present the same picture: there is still a correlation, but it has a much wider dispersion, as one would expect when considering dust reddening.

Nevertheless, there is still room to reconcile these observations. The vast majority of the galaxies from the three ground-based surveys have line fluxes brighter than  $3 \times 10^{-17} \text{ erg s}^{-1} \text{ cm}^{-2}$ , while most of the ob-

jects in the NIRSspec samples are fainter than this limit. Therefore, we surmise that there could be a transition for this relation at around this limit. Future NIRSspec data, when cumulating a sufficient number of objects at the brighter levels, will solve the current discrepancy.

## 5. CONCLUSION

Using a large sample consisting of 251  $R \sim 100$  PRISM spectra and 312  $R \sim 1000$  Grating spectra (totaling 480 unique galaxies) taken by the JWST NIRSspec instrument in three widely separated extragalactic fields, we found a surprisingly tight linear relationship between  $\text{H}\alpha$  and [O III] emission line fluxes (in logarithmic space) that spans a wide redshift range ( $z \sim 1.5 - 7$ ). Such a tight linear correlation is mysterious, as dust reddening would have skewed any intrinsic correlation between the two. From a subsample consisting of 179 PRISM spectra and 265 Grating spectra (378 unique galaxies) that allows the derivation of dust reddening using the “gold standard” Balmer decrement method, we found yet another surprising result: about  $\sim 40\%$  of our objects have  $\text{H}\alpha/\text{H}\beta$  line flux ratios smaller than the canonical Case B value of 2.86, some of which are as small as  $\sim 1.0$ . This casts serious doubts to the universality of the Case B assumption. We show that such non-Case B  $\text{H}\alpha/\text{H}\beta$  ratios are also present in large fractions ( $\sim 30\%$ ) in at least two public JWST NIRSspec catalogs produced by two independent teams as well as in three ground-based redshift surveys carried out at Keck and Subaru. Our finding adds more weight to the challenges to the validity of the Case B assumption recently made by N. Pirzkal et al. (2024) and C. Scarlata et al. (2024), and it is highly likely that the Case B assumption is not universally applicable. This will have a far-reaching impact to our spectral analysis in general. The non-Case B Balmer decrements and the tight  $\text{H}\alpha$ -[O III] correlation call for further theoretical studies to understand the underlying physical mechanisms.

## ACKNOWLEDGMENTS

The authors acknowledge the support from the NSF grant AST-2307447, the NASA grant 80NSSC23K0491 and the University of Missouri Research Council grant URC-23-029. This project is based on observations made with the NASA/ESA/CSA James Webb Space Telescope and obtained from the Mikulski Archive for Space Telescopes, which is a collaboration between the Space Telescope Science Institute (STScI/NASA), the Space Telescope European Coordinating Facility (ST-ECF/ESA), and the Canadian Astronomy Data Centre (CAD/C/NRC/CSA). All the JWST NIRSspec data used in this paper can be found in MAST: [10.17909/mzqy-r528](https://mast.stsci.org/#/api/v0/objects/10.17909/mzqy-r528).

## APPENDIX

Several incidents of non-Case B Balmer decrements have been specifically reported in the literature, but none of these were used to question the validity of the Case B assumption. While studying 24 Ly $\alpha$  emitters at  $z \sim 0.2\text{--}0.3$ , [H. Atek et al. \(2009\)](#) found that a few of them have “negative extinction with large uncertainties” and believed that these could be due to calibration errors, a stronger stellar absorption than assumed, or enhanced H $\beta$  emission from a reflection nebula. [N. A. Reddy et al. \(2015\)](#) measured the Balmer decrements from the early observations of the MOSDEF program and showed that there were a significant number of sources with non-Case B ratios, but this was not further discussed. In their study of “blueberry galaxies” selected from the SDSS, [H. Yang et al. \(2017\)](#) mentioned that most of them (32 out of 41) have non-Case B ratios; however, they attributed this to the poor flat-field calibration at the wavelength range where the H $\alpha$  line locates. Such sporadic discoveries continued into the JWST era. Using the wide-field slitless spectroscopy done by the NIRSS instrument, [J. Matharu et al. \(2023\)](#) investigated spatially resolved Balmer decrements in 117 galaxies by stacking and saw some indications of H $\alpha$  and H $\beta$  line ratio being lower than 2.86 in the inner parts of the galaxies. However, they concluded that such ratios were due to spurious measurements. Two incidents of non-Case B line ratios from the JWST NIRSpec medium-resolution grating data have also been reported. [M. W. Topping et al. \(2024\)](#) studied a metal-poor  $z = 6.1$  galaxy, which has the line ratio of 2.55; they argued that this ratio could still be consistent with the Case B recombination under twice higher electron temperature and two orders of magnitude higher electron density. [A. J. Cameron et al. \(2024\)](#) discussed in detail a  $z = 5.943$  Ly $\alpha$  emitter that has a prominent nebular continuum (this galaxy is in our sample), for which their measured line fluxes give the H $\alpha$ /H $\beta$  ratio of  $\sim 2.65$ . However, they believed that this was due to the underestimated H $\alpha$  flux in their measurement.

## REFERENCES

- Arrabal Haro, P., Dickinson, M., Finkelstein, S. L., et al. 2023, *ApJL*, 951, L22, doi: [10.3847/2041-8213/acdd54](https://doi.org/10.3847/2041-8213/acdd54)
- Atek, H., Kunth, D., Schaerer, D., et al. 2009, *A&A*, 506, L1, doi: [10.1051/0004-6361/200912787](https://doi.org/10.1051/0004-6361/200912787)
- Baldwin, J. A., Phillips, M. M., & Terlevich, R. 1981, *PASP*, 93, 5, doi: [10.1086/130766](https://doi.org/10.1086/130766)
- Bezanson, R., Labbe, I., Whitaker, K. E., et al. 2024, *ApJ*, 974, 92, doi: [10.3847/1538-4357/ad66cf](https://doi.org/10.3847/1538-4357/ad66cf)
- Brammer, G. 2023, 0.6.17 Zenodo, doi: [10.5281/zenodo.7299500](https://doi.org/10.5281/zenodo.7299500)
- Bruzual, G., & Charlot, S. 2003, *MNRAS*, 344, 1000, doi: [10.1046/j.1365-8711.2003.06897.x](https://doi.org/10.1046/j.1365-8711.2003.06897.x)
- Bushouse, H., Eisenhamer, J., Dencheva, N., et al. 2024, 1.14.0 Zenodo, doi: [10.5281/zenodo.6984365](https://doi.org/10.5281/zenodo.6984365)
- Calzetti, D., Armus, L., Bohlin, R. C., et al. 2000, *ApJ*, 533, 682, doi: [10.1086/308692](https://doi.org/10.1086/308692)
- Calzetti, D., Kinney, A. L., & Storchi-Bergmann, T. 1994, *ApJ*, 429, 582, doi: [10.1086/174346](https://doi.org/10.1086/174346)
- Cameron, A. J., Katz, H., Witten, C., et al. 2024, *MNRAS*, 534, 523, doi: [10.1093/mnras/stae1547](https://doi.org/10.1093/mnras/stae1547)
- Carnall, A. C., McLure, R. J., Dunlop, J. S., & Davé, R. 2018, *MNRAS*, 480, 4379, doi: [10.1093/mnras/sty2169](https://doi.org/10.1093/mnras/sty2169)
- D’Eugenio, F., Cameron, A. J., Scholtz, J., et al. 2024, arXiv e-prints, arXiv:2404.06531, doi: [10.48550/arXiv.2404.06531](https://doi.org/10.48550/arXiv.2404.06531)
- Earl, N., Tollerud, E., O’Steen, R., et al. 2024, v1.19.0 Zenodo, doi: [10.5281/zenodo.14042033](https://doi.org/10.5281/zenodo.14042033)
- Eisenstein, D. J., Johnson, B. D., Robertson, B., et al. 2023, arXiv e-prints, arXiv:2310.12340, doi: [10.48550/arXiv.2310.12340](https://doi.org/10.48550/arXiv.2310.12340)
- Figueira, M., Pollo, A., Malek, K., et al. 2022, *A&A*, 667, A29, doi: [10.1051/0004-6361/202141701](https://doi.org/10.1051/0004-6361/202141701)
- Finkelstein, S. L., Bagley, M. B., Arrabal Haro, P., et al. 2025, arXiv e-prints, arXiv:2501.04085, doi: [10.48550/arXiv.2501.04085](https://doi.org/10.48550/arXiv.2501.04085)
- Kashino, D., Silverman, J. D., Sanders, D., et al. 2019, *ApJS*, 241, 10, doi: [10.3847/1538-4365/ab06c4](https://doi.org/10.3847/1538-4365/ab06c4)
- Kennicutt, Jr., R. C. 1998, *ARA&A*, 36, 189, doi: [10.1146/annurev.astro.36.1.189](https://doi.org/10.1146/annurev.astro.36.1.189)
- Kewley, L. J., & Dopita, M. A. 2002, *ApJS*, 142, 35, doi: [10.1086/341326](https://doi.org/10.1086/341326)
- Kewley, L. J., Nicholls, D. C., & Sutherland, R. S. 2019, *ARA&A*, 57, 511, doi: [10.1146/annurev-astro-081817-051832](https://doi.org/10.1146/annurev-astro-081817-051832)
- Kriek, M., Shapley, A. E., Reddy, N. A., et al. 2015, *ApJS*, 218, 15, doi: [10.1088/0067-0049/218/2/15](https://doi.org/10.1088/0067-0049/218/2/15)
- Kroupa, P. 2001, *MNRAS*, 322, 231, doi: [10.1046/j.1365-8711.2001.04022.x](https://doi.org/10.1046/j.1365-8711.2001.04022.x)
- Maiolino, R., Nagao, T., Grazian, A., et al. 2008, *A&A*, 488, 463, doi: [10.1051/0004-6361:200809678](https://doi.org/10.1051/0004-6361:200809678)
- Matharu, J., Muzzin, A., Sarrouh, G. T. E., et al. 2023, *ApJL*, 949, L11, doi: [10.3847/2041-8213/acd1db](https://doi.org/10.3847/2041-8213/acd1db)
- Moustakas, J., Kennicutt, Jr., R. C., & Tremonti, C. A. 2006, *ApJ*, 642, 775, doi: [10.1086/500964](https://doi.org/10.1086/500964)

- Nanayakkara, T., Glazebrook, K., Kacprzak, G. G., et al. 2016, *ApJ*, 828, 21, doi: [10.3847/0004-637X/828/1/21](https://doi.org/10.3847/0004-637X/828/1/21)
- Osterbrock, D. E. 1989, *Astrophysics of gaseous nebulae and active galactic nuclei*
- Pirzkal, N., Rothberg, B., Papovich, C., et al. 2024, *ApJ*, 969, 90, doi: [10.3847/1538-4357/ad429c](https://doi.org/10.3847/1538-4357/ad429c)
- Price, S. H., Bezanson, R., Labbe, I., et al. 2024, arXiv e-prints, arXiv:2408.03920, doi: [10.48550/arXiv.2408.03920](https://doi.org/10.48550/arXiv.2408.03920)
- Reddy, N. A., Kriek, M., Shapley, A. E., et al. 2015, *ApJ*, 806, 259, doi: [10.1088/0004-637X/806/2/259](https://doi.org/10.1088/0004-637X/806/2/259)
- Scarlata, C., Hayes, M., Panagia, N., et al. 2024, arXiv e-prints, arXiv:2404.09015, doi: [10.48550/arXiv.2404.09015](https://doi.org/10.48550/arXiv.2404.09015)
- Sun, B., & Yan, H. 2025, arXiv e-prints, arXiv:2502.05751, doi: [10.48550/arXiv.2502.05751](https://doi.org/10.48550/arXiv.2502.05751)
- Suzuki, T. L., Kodama, T., Sobral, D., et al. 2016, *MNRAS*, 462, 181, doi: [10.1093/mnras/stw1655](https://doi.org/10.1093/mnras/stw1655)
- Topping, M. W., Stark, D. P., Senchyna, P., et al. 2024, *MNRAS*, 529, 3301, doi: [10.1093/mnras/stae682](https://doi.org/10.1093/mnras/stae682)
- Villa-Vélez, J. A., Buat, V., Theulé, P., Boquien, M., & Burgarella, D. 2021, *A&A*, 654, A153, doi: [10.1051/0004-6361/202140890](https://doi.org/10.1051/0004-6361/202140890)
- Wen, R., An, F., Zheng, X. Z., et al. 2022, *ApJ*, 933, 50, doi: [10.3847/1538-4357/ac7392](https://doi.org/10.3847/1538-4357/ac7392)
- Yang, H., Malhotra, S., Rhoads, J. E., & Wang, J. 2017, *ApJ*, 847, 38, doi: [10.3847/1538-4357/aa8809](https://doi.org/10.3847/1538-4357/aa8809)